Chinese Physics B

PAPER

Epitaxial synthesis and electronic properties of monolayer Pd_2Se_3*

To cite this article: Peng Fan *et al* 2020 *Chinese Phys. B* **29** 098102

Epitaxial synthesis and electronic properties of monolayer Pd_2Se_3*

Peng Fan(范朋)[1,†], Rui-Zi Zhang(张瑞梓)[1,†], Jing Qi(戚竞)[1,†], En Li(李恩)[1], Guo-Jian Qian(钱国健)[1], Hui Chen(陈辉)[1], Dong-Fei Wang(王东飞)[1], Qi Zheng(郑琦)[1], Qin Wang(汪琴)[1], Xiao Lin(林晓)[1,2], Yu-Yang Zhang(张余洋)[1,2], Shixuan Du(杜世萱)[1,2,‡], Hofer W A[1,3], and Hong-Jun Gao(高鸿钧)[1,2,§]

[1] *Institute of Physics and University of Chinese Academy of Sciences, Chinese Academy of Sciences (CAS), Beijing* 100190, *China*
[2] *CAS Center for Excellence in Topological Quantum Computation, Beijing* 100190, *China*
[3] *School of Natural and Environmental Sciences, Newcastle University, Newcastle upon Tyne Ne77RU, UK*

(Received 21 May 2020; revised manuscript received 15 July 2020; accepted manuscript online 1 August 2020)

Two-dimensional (2D) materials received large amount of studies because of the enormous potential in basic science and industrial applications. Monolayer Pd_2Se_3 is a fascinating 2D material that was predicted to possess excellent thermoelectric, electronic, transport, and optical properties. However, the fabrication of large-scale and high-quality monolayer Pd_2Se_3 is still challenging. Here, we report the synthesis of large-scale and high-quality monolayer Pd_2Se_3 on graphene-SiC (0001) by a two-step epitaxial growth. The atomic structure of Pd_2Se_3 was investigated by scanning tunneling microscope (STM) and confirmed by non-contact atomic force microscope (nc-AFM). Two subgroups of Se atoms have been identified by nc-AFM image in agreement with the theoretically predicted atomic structure. Scanning tunneling spectroscopy (STS) reveals a bandgap of 1.2 eV, suggesting that monolayer Pd_2Se_3 can be a candidate for photoelectronic applications. The atomic structure and defect levels of a single Se vacancy were also investigated. The spatial distribution of STS near the Se vacancy reveals a highly anisotropic electronic behavior. The two-step epitaxial synthesis and characterization of Pd_2Se_3 provide a promising platform for future investigations and applications.

Keywords: 2D material, Pd_2Se_3, scanning tunneling microscope/spectroscopy, non-contact atomic force microscope

PACS: 81.15.–z, 68.55.–a, 71.22.+i, 68.37.Ef **DOI:** 10.1088/1674-1056/abab80

1. Introduction

Two-dimensional (2D) materials with unique properties have generated a vast body of research into applications in nanoscale electronics, thermoelectric devices, and optoelectronics devices.[1–10] Among the large 2D family, transition metal selenides attract much attention because of the excellent electronic properties and potential applications in nanoscale devices.[11–19] Recently, Lin *et al*. reported the fabrication of a new Pd_2Se_3 2D phase,[20] which has never been discovered before. The following theoretical calculations predicted that monolayer Pd_2Se_3 is a good thermoelectric material. It has a small lattice thermal conductivities k_L and high power-factor because of the complex crystal structure formed by $[Se_2]^{2-}$ dimers, Se^{2-} anions, and Pd^{2+} cations coordinated in a square-planar manner.[21] It is also predicted that monolayer Pd_2Se_3 has good carrier mobility comparable to MoS_2 and anisotropic transport properties.[22,23] Due to its excellent physical properties, monolayer Pd_2Se_3 is a very promising candidate for thermoelectrics, anisotropic optoelectronics, and electronic devices.

As there is no layered bulk parent,[20] monolayer Pd_2Se_3 cannot be obtained by mechanical exfoliation. Until now, monolayer Pd_2Se_3 with a scale of several nanometers has only been fabricated by transforming bilayer $PdSe_2$ using a microscope's electron beam, which has been analyzed by scanning transmission electron microscopy (STEM).[20,24,25] In this synthesized method, the mix of Pd_2Se_3 and $PdSe_2$ impedes the investigation and application of monolayer Pd_2Se_3, hence the fabrication of large-scale and high-quality monolayer Pd_2Se_3 is required. Moreover, an investigation of related physical/electronic properties is still missing.

Motivated by the electron beam induced transformation from bilayer $PdSe_2$ to monolayer Pd_2Se_3, we designed a two-step thermal-annealing procedure to fabricate monolayer Pd_2Se_3. We first synthesized bilayer $PdSe_2$ on a graphene-SiC (0001) substrate in a selenium-rich atmosphere (the ratio of Pd and Se is 1:10). Then, monolayer Pd_2Se_3 with a scale of tens of nanometers was fabricated by annealing the bilayer $PdSe_2$ in a selenium-deficient atmosphere (no selenium was

*Project supported by the National Key Research and Development Program of China (Grant Nos. 2016YFA0202300, 2018YFA0305800, and 2019YFA0308500), the National Natural Science Foundation of China (Grant Nos. 51922011, 51872284, and 61888102), the Strategic Priority Research Program of the Chinese Academy of Sciences (Grant Nos. XDB30000000 and XDB28000000), and the Science Fund from University of the Chinese Academy of Sciences.

†These authors contributed equally to this work.
‡Corresponding author. E-mail: sxdu@iphy.ac.cn
§Corresponding author. E-mail: hjgao@iphy.ac.cn

deposited). The atomic structure of the as-fabricated monolayer Pd_2Se_3 was then investigated by a combination of low-temperature scanning tunneling microscope/spectroscopy (LT-STM/S), non-contact atomic force microscope (nc-AFM), and density functional theory (DFT) calculations. By employing STS at 4 K, a bandgap of 1.2 eV in the basal plane of monolayer Pd_2Se_3 was revealed. Se vacancies were also explored by combining LT-STM, nc-AFM, and density functional theory (DFT) calculations. It is found that the vacancy is formed by the disappearance of one Se atom of a $[Se_2]^{2-}$ dimer and rebounding of the other Se atom with four neighboring Pd atoms. Three defect states at different energies have been explored. The spatially resolved STS indicates that the defect state near the valance band is anisotropic in different crystal directions.

2. Methods

2.1. Sample preparation and characterization

The sample was synthesized by molecular beam epitaxy in a commercial ultrahigh vacuum (UHV) STM system with a base pressure of 2.0×10^{-10} mbar (1 bar $= 10^5$ Pa). A nitrogen-doped 6H–SiC (0001) was flashed to 1550 K, leading to a graphene terminated surface.[26,27] The atomic beams of Pd (99.95%, Alfa Aesar) and Se (99.999%, Alfa Aesar) were simultaneously deposited at a ratio of $\sim 1:10$ with the substrate maintained at 500 K.[28] Before UHV LT-STM/STS (UNISOKU) measurements, the sample was annealed at 475 K for 30 minutes. Differential conductance ($\mathrm{d}I/\mathrm{d}V$) spectra were acquired by a standard lock-in amplifier at a frequency of 973.1 Hz with a 20-mV rms modulation. The tip calibration were performed on an Au (111) substrate. All nc-AFM measurements were performed using a commercial qPlus tuning fork sensor in frequency modulation mode with a CO-terminated Pt/Ir tip.[29] The resonance frequency was about 27.9 kHz, and stiffness about 1800 N/m. The resonance amplitude was 0.1 nm. The imaging heights for all nc-AFM measurements were -4.5 Å referred to the STM tunneling junction height ($V_s = -2$ V and $I_t = 10$ pA) on Pd_2Se_3 substrate.

2.2. First-principle calculations

First-principle calculations were performed within the Vienna *ab initio* simulation package (VASP),[30] version 5.4.1, using the projector augmented-wave (PAW) method.[31] Electron exchange and correlation effects were treated using generalized gradient approximation (GGA) in the form of Perdew–Burke–Ernzerhof (PBE).[32] The STM simulations were based on the Tersoff–Hamann approximation.[33] Within this approximation, the STM image was a contour of the local density of states (LDOS) of the system. In the calculation of monolayer Pd_2Se_3, a vacuum layer of 25 Å was used and all atoms were relaxed until the net force on every atom was smaller than 0.01 eV/Å. The energy cutoff of the plane-wave basis set was 400 eV, and a $21 \times 21 \times 1$ Monkhost–Pack k-point mesh was used to sample the Brillouin zone. To model the effect of defects on the surface, a $4 \times 4 \times 1$ supercell structure of the optimized monolayer Pd_2Se_3 was considered, and then a single Se vacancy was introduced on Pd_2Se_3 layer. For both pristine and defective supercell structures, $3 \times 3 \times 1$ k-point samplings were used, and the atoms were relaxed until the residual forces were below 0.01 eV/Å. The structure figures were produced with VESTA.

3. Results and discussion

The fabrication process of monolayer Pd_2Se_3 is shown schematically in Fig. 1(a). Firstly, bilayer or monolayer graphene was formed on a nitrogen-doped SiC (0001) by flashing the substrate to 1550 K. Then, palladium (Pd) and selenium (Se) were deposited at a ratio of 1 to 10 on graphene/SiC (0001) whose temperature was kept at 500 K, resulting in the successful fabrication of bilayer $PdSe_2$ (middle panel of Fig. 1(a)).[28] The sample was further annealed at 475 K for 30 minutes. As the second round of annealing was processed in a selenium-deficient atmosphere, the emergence of Se vacancies results in the decreasing of interlayer distance, the merging of bilayer $PdSe_2$ and finally the formation of Pd_2Se_3 as shown in the lower panel of Fig. 1(a). Figure 1(b) shows a large scale and high-quality monolayer Pd_2Se_3 island on bilayer-graphene/SiC. The line profile in the inset of Fig. 1(b) indicates that the height of the step edge is 7.7 Å. Figure 1(c) shows an atomically resolved STM image obtained after the second-round annealing process in a selenium-deficient atmosphere. The blue box in Fig. 1(c) indicates one unit cell with $a = 0.6$ nm and $b = 0.61$ nm. The neighboring elliptical protrusions form dimers in b direction. The inset shows the simulated STM image, which is consistent to the experimental results. The line profile across the patterns presented in the lower panel of Fig. 1(c) clearly shows the formation of the dimers.

To study the stability of as-grown Pd_2Se_3, we covered the sample with Se layers in the vacuum condition and exposed it in air for 30 minutes. Then we loaded it back to vacuum chamber and annealed it at 475 K for 20 minutes. The STM image shows similar features to the ones in the STM image obtained before air exposure, indicating that the Se layer-covered Pd_2Se_3 is chemically stable in air.

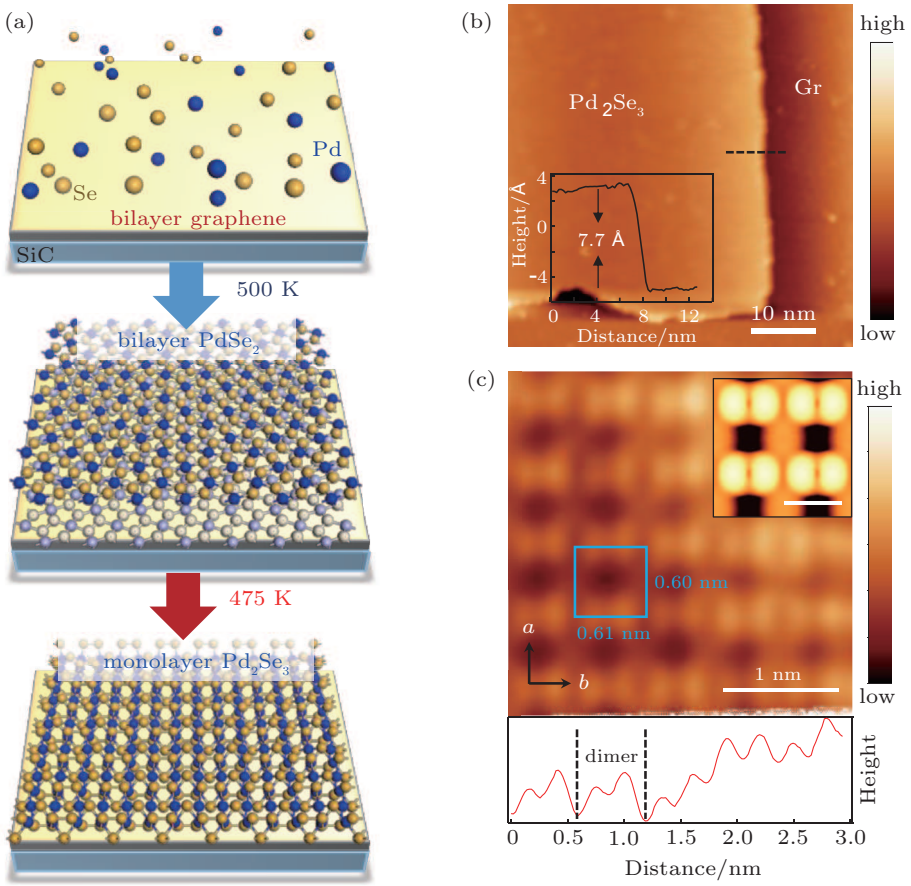

Fig. 1. Schematic diagrams of the fabrication process of monolayer Pd_2Se_3 and STM images. (a) The schematic diagram of the fabrication process. Firstly, Pd and Se atoms were deposited simultaneously with the substrate maintained at 500 K for 10 minutes (top panel). Bilayer $PdSe_2$ was fabricated (middle panel). After annealed at selenium-deficient atmosphere, monolayer Pd_2Se_3 was successfully synthesized (bottom panel). (b) A large scale STM image ($V_s = -1$ V, $I_t = 10$ pA) of Pd_2Se_3. The inset is the line-profile cross the step edge, highlighted by the black dashed line. (c) A zoom-in STM image ($V_s = -1$ V, $I_t = 100$ pA) of Pd_2Se_3 and line-profile cross the patterns. The inset shows simulated STM image ($V_s = -0.8$ V). Scale bar: 0.5 nm. The lattice constants are 0.60 nm in a direction and 0.61 nm in b direction.

To confirm that the as-fabricated material is monolayer Pd_2Se_3, we characterized the layer with nc-AFM. Figure 2(a) is an atomically resolved AFM image. The unit cell is highlighted by a blue box with lattice constants $a = 0.6$ nm and $b = 0.61$ nm, which are the same as that shown in Fig. 1(c). Figure 2(b) shows the top-view, side-view, and front-view of atomic structure of Pd_2Se_3. The lattice constants, $a = 0.595$ nm and $b = 0.615$ nm,[22] agree well with our observations from the STM and nc-AFM images. From the top-view in Fig. 2(b), we found that the Se atoms in the top layer can be distinguished by two groups, the Se atoms in yellow (labeled as Se_A) form dimer structures, while those in orange (labeled as Se_B) distribute dispersedly. From the side view and front view, it is clearly seen that the yellow ones are slightly higher than the orange ones. As nc-AFM can resolve all the top-layer Se atoms, we superimpose the top-layer Se atoms of Pd_2Se_3 onto the AFM image. The nc-AFM image exhibits two groups of protrusions that are clearly resolved by different brightness. Since the brightness corresponds to the height of an atom, the brighter protrusions are slightly higher in position than the others. The brighter protrusions exhibit dimer patterns similar to that observed in the STM image (Fig. 1(c)), corresponding to the dimerization of neighboring Se atoms in the top layer with higher position (yellow balls). Moreover, the Se atoms in the top layer with lower positions, not clearly enough in STM image (Fig. 1(c)), are seen in Fig. 2(a) with less brightness, corresponding to the orange balls. Therefore, by combining nc-AFM image with DFT calculation, we demonstrate that the material we fabricated is monolayer Pd_2Se_3. DFT calculations also reveal that there is significant difference between the Raman frequencies of monolayer $PdSe_2$ and monolayer Pd_2Se_3,[23] which means that Raman spectrum can be used to distinguish these two materials in the future.

The electronic structure of monolayer Pd_2Se_3 was investigated by combining low-temperature STS and DFT calculations. The dI/dV spectrum was collected on the perfect plane of monolayer Pd_2Se_3, as shown in Fig. 2(c). The valence band maximum (VBM) and conductance band minimum (CBM) are indicated by red dashed lines. The bandgap is ~ 1.2 eV. The blue line in Fig. 2(c) is the calculated density of state (DOS) of monolayer Pd_2Se_3 using a hybrid functional (see the method section), which agrees well with the experimental observation.

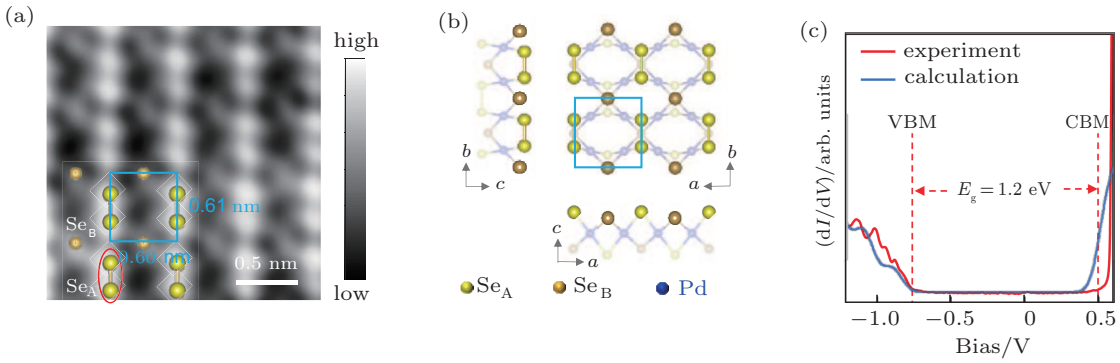

Fig. 2. The atomic structure and electronic properties of monolayer Pd_2Se_3. (a) A high-resolution AFM image ($A = 100$ pm, $Z = -4.5$ Å) of monolayer Pd_2Se_3. A model of the topmost layer is superimposed on the image. The red ellipse highlights Se–Se dimer, which is higher than undimerized Se atoms. (b) Side-view, top-view, and front-view of monolayer Pd_2Se_3. (c) dI/dV spectra (red line ($V_s = -1$ V, $I_t = 100$ pA)) and the calculated density of states (blue line) of monolayer Pd_2Se_3.

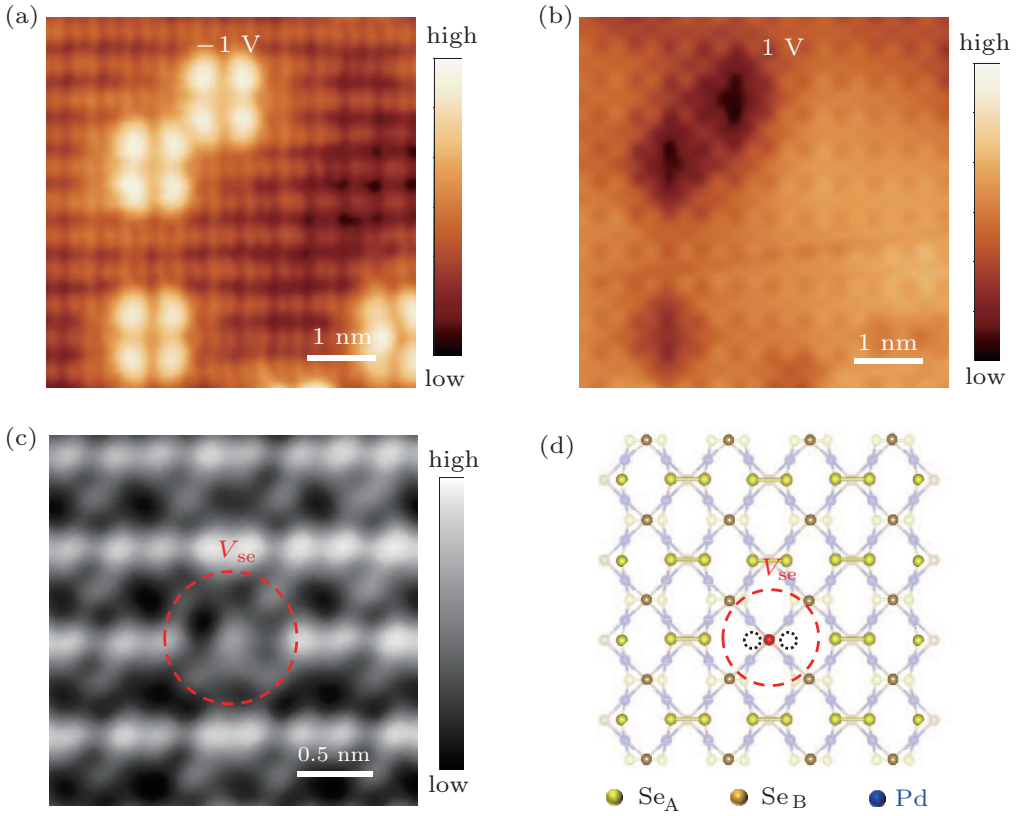

Fig. 3. The atomic structure of the Se vacancy in monolayer Pd_2Se_3. (a) and (b) The STM images ($I_t = 100$ pA) of Se vacancies at the sample bias voltages of −1 V and 1 V, respectively. The butterfly-like and pitlike structures are Se vacancies. (c) An atomic-resolution AFM image ($A = 100$ pm, $Z = -4.5$ Å) containing a Se vacancy. The red dashed circle highlights one Se vacancy. (d) DFT calculated structure of a Se vacancy. The red dashed circle corresponds to the one shown in panel (c). The black dashed circles indicate the Se–Se dimer before Se vacancy forms. When one of the Se atoms disappears, the other moves to the position of the red dot and binds to the four neighboring Pd atoms.

It has been reported that point defects may have a strong effect on the thermoelectric efficiency.[34,35] So, we investigated the atomic structures and electronic structures of Se vacancies. We produced Se vacancies by annealing the as-grown sample at 475 K in the vacuum for more than twenty hours. Figures 3(a) and 3(b) are STM images of Se vacancies at negative and positive sample bias, respectively. The STM image of Se vacancies exhibits four-fold flower-like electronic states at negative bias (Fig. 3(a)) and dark holes at positive bias (Fig. 3(b)). Figure 3(c) is the nc-AFM image of a single Se vacancy highlighted by the dashed red circle. It is clearly seen that one Se atom in a dimer disappears, while the other Se atom in the dimer moves to the high-symmetric site. The theoretically optimized atomic structure shown in Fig. 3(d) indicates that after losing one Se atom in a Se–Se dimer (dashed black circles), the other Se atom moves to the high-symmetric site and rebound with four neighboring Pd atoms. This structure has the lowest energy and agrees well with the one in nc-

AFM measurements.

By measuring the spatial distribution of the dI/dV spectra, the anisotropic electronic properties of Se vacancies were revealed. The waterfall plots of the dI/dV spectra along the green and red arrows in Fig. 4(a) are shown in Figs. 4(b) and 4(c), respectively. There are three main defect states, labeled by grey (P_1), green (P_2), and blue (P_3) dashed lines in Fig. 4(b) and Fig. 4(c). It is found that the P_2 and P_3 always decay simultaneously in both directions, with a decay length of 1.5 nm, while the P_1 shows a highly anisotropic behaviors in the two directions. It has a larger spatial extension (~ 2.4 nm) in the direction of the green arrow in Fig. 4(a). The P_1 state exists in each spectrum as displayed in Fig. 4(b), respectively. In contrast, the P_1 decays fast in the direction of the red arrow shown in Fig. 4(a) and extends only 1.5 nm, as shown in Fig. 4(c).

The spatial distribution of the defect state P_1 was also investigated. The dI/dV map of the P_1 state is shown in Fig. 4(d). The corresponding topographic STM image is highlighted by the blue dashed rectangle of Fig. 4(a). The dI/dV map shows a one-dimensional elliptic pattern extended in b direction. The pattern is similar to the patterns in STM images. The spatial decay of this defect state indicates highly anisotropic electronic properties of monolayer Pd_2Se_3.

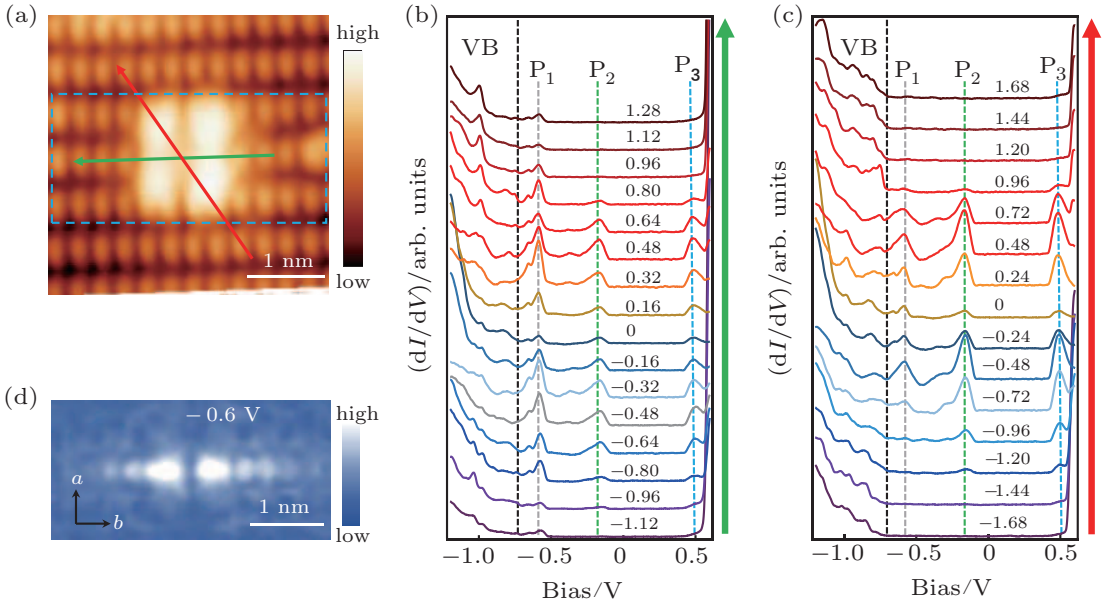

Fig. 4. Electronic properties of Se vacancy. (a) An STM image ($V_s = -1$ V, $I_t = 10$ pA) of Se vacancy. (b) and (c) Waterfall plots of a period normalized STS ($V_s = -1$ V, $I_t = 100$ pA) along the green arrow and the red arrow in panel (a), respectively. The black dashed lines indicate the gap edge at the valance band. P_1 (the grey dashed line), P_2 (the green dashed line), and P_3 (the blue dashed line) indicate three main defect levels. (d) The dI/dV map ($V_s = -1$ V, $I_t = 100$ pA) at -0.6 V of Se vacancy. The corresponding region is highlighted by dashed blue box in panel (a).

4. Conclusion

In summary, large-scale and high-quality monolayered Pd_2Se_3 islands were successfully synthesized on graphene-SiC (0001) by epitaxial growth. By combining STM, nc-AFM, and DFT calculations, the atomic structure of monolayer Pd_2Se_3 was revealed. The spectroscopy shows a band gap of 1.2 eV, which is suitable for absorber materials in ultrathin photovoltaic devices. The STM images of Se vacancies show different features at different sample bias voltages. Further nc-AFM measurements and DFT calculations reveal the configuration of the Se vacancy. The dI/dV spectra and map show that the vacancy state is highly anisotropic. With a suitable band gap size and anisotropic electronic properties, monolayer Pd_2Se_3 may offer a potential platform for thin-film electronics, infrared optoelectronics, and novel devices in which anisotropic properties are desirable.

References

[1] Wang Q H, Kalantar-Zadeh K, Kis A, Coleman J N and Strano M S 2012 *Nat. Nanotechnol.* **7** 699
[2] Kumar S and Schwingenschlögl U 2015 *Chem. Mater.* **27** 1278
[3] Li E, Zhang R Z, Li H, Liu C, Li G, Wang J O, Qian T, Ding H, Zhang Y Y, Du S X, Lin X and Gao H J 2018 *Chin. Phys. B* **27** 086804
[4] Tan C, Cao X, Wu X J, He Q, Yang J, Zhang X, Chen J, Zhao W, Han S, Nam G H, Sindoro M and Zhang H 2017 *Chem. Rev.* **117** 6225
[5] Novoselov K S, Mishchenko A, Carvalho A and Castro Neto A H 2016 *Science* **353** aac9439
[6] Chen S and Shi G 2017 *Adv. Mater.* **29** 1605448
[7] Qian K, Gao L, Li H, Zhang S, Yan J H, Liu C, Wang J O, Qian T, Ding H, Zhang Y Y, Lin X, Du S X and Gao H J 2020 *Chin. Phys. B* **29** 018104
[8] Zeng Y, Zhang S, Li X, Ao J, Sun Y, Liu W, Liu F, Gao P and Zhang Y 2019 *Chin. Phys. B* **28** 058101
[9] Zhang S, Song Y, Li H, Li J M, Qian K, Liu C, Wang J O, Qian T, Zhang Y Y, Lu J C, Ding H, Lin X, Pan J, Du S X and Gao H J 2020 *Chin. Phys. Lett.* **37** 068103
[10] Geim A K and Grigorieva I V 2013 *Nature* **499** 419
[11] Wu J, Schmidt H, Amara K K, Xu X, Eda G and Ozyilmaz B 2014 *Nano Lett.* **14** 2730
[12] Yoshida M, Iizuka T, Saito Y, Onga M, Suzuki R, Zhang Y, Iwasa Y and Shimizu S 2016 *Nano Lett.* **16** 2061

[13] Lu J, Bao D L, Qian K, Zhang S, Chen H, Lin X, Du S X and Gao H J 2017 *ACS Nano* **11** 1689
[14] Liu Z L, Lei B, Zhu Z L, Tao L, Qi J, Bao D L, Wu X, Huang L, Zhang Y Y, Lin X, Wang Y L, Du S, Pantelides S T and Gao H J 2019 *Nano Lett.* **19** 4897
[15] Liu H, Bao L, Zhou Z, Che B, Zhang R, Bian C, Ma R, Wu L, Yang H, Li J, Gu C, Shen C M, Du S and Gao H J 2019 *Nano Lett.* **19** 4551
[16] Yang S Z, Sun W, Zhang Y Y, Gong Y, Oxley M P, Lupini A R, Ajayan P M, Chisholm M F, Pantelides S T and Zhou W 2019 *Phys. Rev. Lett.* **122** 106101
[17] Gao L, Sun J T, Lu J C, Li H, Qian K, Zhang S, Zhang Y Y, Qian T, Ding H, Lin X, Du S and Gao H J 2018 *Adv. Mater.* **30** 1707055
[18] Liang Q, Wang Q, Zhang Q, Wei J, Lim S X, Zhu R, Hu J, Wei W, Lee C, Sow C, Zhang W and Wee A T S 2019 *Adv. Mater.* **31** 1807609
[19] Oyedele A D, Yang S, Feng T, Haglund A V, Gu Y, Puretzky A A, Briggs D, Rouleau C M, Chisholm M F, Unocic R R, Mandrus D, Meyer H M, Pantelides S T, Geohegan D B and Xiao K 2019 *J. Am. Chem. Soc.* **141** 8928
[20] Lin J, Zuluaga S, Yu P, Liu Z, Pantelides S T and Suenaga K 2017 *Phys. Rev. Lett.* **119** 016101
[21] Naghavi S S, He J, Xia Y and Wolverton C 2018 *Chem. Mater.* **30** 5639
[22] Zhu X, Li F, Wang Y, Qiao M and Li Y 2018 *J. Mater. Chem. C* **6** 4494
[23] Li X, Zhang S, Guo Y, Wang F Q and Wang Q 2018 *Nanomaterials (Basel)* **8** 832
[24] Chen J, Ryu G H, Sinha S and Warner J H 2019 *ACS Nano* **13** 8256
[25] Ryu G H, Zhu T, Chen J, Sinha S, Shautsova V, Grossman J C and Warner J H 2019 *Adv. Mater.* **31** 1904251
[26] Wang Q, Zhang W, Wang L, He K, Ma X and Xue Q 2013 *J. Phys.: Condens. Matter* **25** 095002
[27] Riedl C, Starke U, Bernhardt J, Franke M and Heinz K 2007 *Phys. Rev. B* **76** 245406
[28] Li E, Wang D, Fan P, Zhang R, Zhang Y Y, Li G, Mao J, Wang Y, Lin X, Du S X and Gao H J 2018 *Nano Res.* **11** 5858
[29] Bartels L, Meyer G and Rieder K H 1997 *Appl. Phys. Lett.* **71** 213
[30] Kresse G and Furthmüller J 1996 *Phys. Rev. B* **54** 11169
[31] Blöchl P E 1994 *Phys. Rev. B* **50** 17953
[32] Perdew J P, Burke K and Ernzerhof M 1996 *Phys. Rev. Lett.* **77** 3865
[33] Tersoff J and Hamann D R 1985 *Phys. Rev. B* **31** 805
[34] Toberer E S, Zevalkink A and Snyder G J 2011 *J. Mater. Chem.* **21** 15843
[35] Poudel B, Hao Q, Ma Y, Lan Y, Minnich A, Yu B, Yan X, Wang D, Muto A and Vashaee D 2008 *Science* **320** 634